

# Small scale star formation as revealed by VVVX galactic cluster candidates.

J. Borissova,<sup>1,2</sup>★ R. Kurtev,<sup>1,2</sup> N. Amarinho,<sup>3</sup> J. Alonso-García,<sup>4,2</sup> S. Ramírez Alegría,<sup>4</sup>, S. Bernal,<sup>1,2</sup> N. Medina,<sup>1,2</sup> A.-N. Chené,<sup>5</sup> V. D. Ivanov,<sup>6</sup> P.W. Lucas,<sup>7</sup> and D. Minniti<sup>8</sup>

<sup>1</sup>*Instituto de Física y Astronomía, Universidad de Valparaíso, Av. Gran Bretaña 1111, Playa Ancha, Casilla 5030, Chile.*

<sup>2</sup>*Millennium Institute of Astrophysics (MAS), Santiago, Chile.*

<sup>3</sup>*Laboratório Nacional de Astrofísica (LNA) - Brazil*

<sup>4</sup>*Centro de Astronomía (CITEVA), Universidad de Antofagasta, Avenida Angamos 601, Antofagasta, Chile*

<sup>5</sup>*NOIRLab international Gemini Observatory, Northern Operations Center, 670 A'ohoku Place, Hilo, HI 96720, USA*

<sup>6</sup>*European Southern Observatory, Karl Schwarzschildstr. 2, D-85748 Garching bei München, Germany*

<sup>7</sup>*Centre for Astrophysics, University of Hertfordshire, College Lane, Hatfield, AL10 9AB, UK.*

<sup>8</sup>*Departamento de Física, Facultad de Ciencias Exactas, Universidad Andrés Bello, Av. Fernandez Concha 700, Las Condes, Santiago, Chile.*

Accepted XXX. Received YYY; in original form ZZZ

## ABSTRACT

We report a search and analysis of obscured cluster candidates in the “VISTA Variables in the Via Lactea eXtended (VVVX)” ESO Public Survey area encompassing the region between  $229^{\circ}.4 < l < 295^{\circ}.2$  and  $-4^{\circ}.3 < b < 4^{\circ}.4$  of the southern Galactic disk. We discover and propose 88 new clusters. We improve the completeness of the embedded cluster population in this region, adding small size (linear diameters of 0.2–1.4 pc) and relatively far objects (heliocentric distance between 2 and 4 kpc) to existing catalogues. Nine candidates are proposed to be older open cluster candidates. Three of them (VVVX CL 204, 207, 208) have sufficient numbers of well-resolved stellar members to allow us to determine some basic cluster parameters. We confirm their nature as older, low-mass open clusters. Photometric analysis of 15 known clusters shows that they have ages above 20 Myr, and masses below  $2000 M_{\odot}$ : in general, their proper motions follow the motion of the disk. We outline some groups of clusters, most probably formed within the same dust complex. Broadly, our candidates follow the network of filamentary structure in the remaining dust. Thus, in this part of the southern disk of the Galaxy, we have found recent star formation, producing small size and young clusters, in addition to the well known, massive young clusters, including NGC 3603, Westerlund 2 and the Carina Nebula Complex.

**Key words:** Galaxy: open clusters and associations – Galaxy: disk –Infrared: stars

## 1 INTRODUCTION

The investigation of open star clusters has been very useful for the exploration of the disk of our own Milky Way. They are excellent laboratories not only for stellar evolution theory, but also to test the star formation history and the structure of the Galactic disk (e.g. [Moitinho 2010](#)).

This is an active area of research where good progress is being made. In the optical regime, the Gaia mission has enabled discovery of hundreds of cluster candidates, reviewed known clusters and distinguished asterisms among objects previously reported as stellar clusters (e.g. [Cantat-Gaudin](#)

[et al. 2018, 2019](#) and [Cantat-Gaudin & Anders 2020; Gran et al. 2019](#)). The near-infrared data allow access to more embedded and younger objects, completing the view obtained through optical data. The early discoveries done with the 2 MASS survey (e.g. [Bica et al. 2003; Dutra et al. 2003; Froebrich et al. 2007](#)) have been recently complemented with VVV survey data (e.g. [Borissova et al. 2011, 2014, 2018; Solin et al. 2014; Barbá et al. 2015; Ivanov et al. 2017](#); and references therein) through a variety of techniques. The future searches with Gaia DR3 and the LSST are also expected to yield large numbers of open clusters (e.g. The LSST Science Book, [LSST Science Collaboration 2009](#)).

The characterization of these open cluster candidates is often tricky, as they are located at low Galactic latitudes where not only the stellar density is high, but also the in-

★ Based on observations gathered with VIRCAM at the ESO VISTA telescope, as part of observing programs 198.B-2004.

terstellar extinction and reddening are problematic. It is not surprising that different approaches have been taken to measure the physical parameters for these clusters, often using vastly different datasets. Fortunately, the large datasets now available allow us to shift from the analysis of single objects to the study of large samples like the ones produced now by Gaia and VVV, and also LSST in the future. In particular, we can now try to trace the star formation patterns at different scales across the Galactic disk.

The near-IR offers advantages over optical wavelengths for these kinds of studies because it is less sensitive to reddening and extinction. Using the near-IR we can see for example, young, obscured clusters farther away, deeper into the Galactic plane, and can also measure more accurate distances, that are less affected by reddening uncertainties. There is a disadvantage, however: the background contamination in the near-IR is generally much larger than in the optical, because at shorter wavelengths the same extinction helps to reduce the numbers of distant stars that can be detected. Thus, the optical color magnitude diagrams of nearby clusters often appear cleaner than the more distant ones that we are finding in the near-IR. Therefore, both optical and near-IR studies are worthwhile and complementary.

In this work we take advantage of the near-IR VVVX survey, searching for distant ( $1.0 < D(\text{kpc}) < 10.0$ ) young clusters at very low Galactic latitudes ( $-5^\circ < b < +5^\circ$ ) and use them to trace small scale star formation across their fields. This is the fourth paper in our effort to study the obscured cluster population in the MW (Borissova et al. 2011, 2014, 2018), using the “VISTA Variables in the Vía Láctea” (VVV) and the new “VVV eXtended” (VVVX) surveys that cover  $\sim 1700 \text{ deg}^2$  of the inner MW bulge and southern disk in  $ZYJHK_S$  bands (Minniti et al. 2010; Saito et al. 2012). The VVV/VVVX images have a pixel size of  $0.34''$ , smaller than 2MASS (Two Micron All Sky Survey; Skrutskie et al. 2006), GLIMPSE (Galactic Legacy Infrared Mid-Plane Survey Extraordinaire; Benjamin et al. 2003) and WISE (Wide-field Infrared Survey Explorer, Wright et al. 2010) – especially important for searching of small/compact cluster candidates. This allows us to investigate the formation of such objects and to connect them with the dust distribution, obtained with the mid-IR observations.

Here we expand our search into regions recently observed by the VVVX survey (Fig. 1): two slices away from the plane in the southern disk ( $65^\circ \times 4^\circ$ , tiles from e601 to e729 and from e767 to e895; lower and upper part, marked in blue) and an extension along the mid-plane ( $65^\circ \times 4^\circ$ , tiles from e1001 to e1180; shown in yellow). The analyzed area encompass the region between  $229.4 < l < 295.2$  and  $-4.3 < b < 4.4$ . A description of the survey data is included in Section 2. Sections 3 and 4 detail the candidate detection methods and validation. Section 5 summarizes our review of known clusters in the search area, reported by Bica et al. (2019). The spatial distribution of clusters with distance determination, identifying several groups and structures, is discussed in Section 6.

## 2 SURVEY DATA

The VVVX survey was launched in 2016 as an extension of the completed VVV survey in order to enhance its legacy

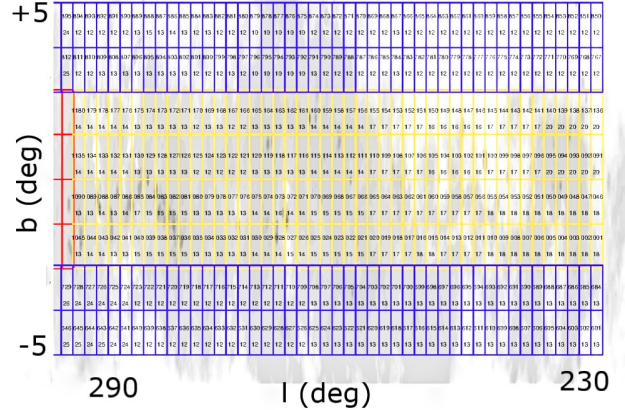


**Figure 1.** The VVVX Survey area, investigated in this work. The blue and yellow squares show the VVVX outer disk fields. The numbers in each tile are its identification number (top) and the number of available  $K_S$  epochs, as of May 2, 2019.

value. The VVVX provides a spatial coverage from  $l=230^\circ$  to  $l=20^\circ$  ( $7^h < \alpha < 19^h$ ). The data were obtained with the 4.1-meter ESO VISTA telescope (Visual and Infrared Survey Telescope for Astronomy; Emerson, McPherson & Sutherland 2006) located at Cerro Paranal, Chile, with the 16-detector VIRCAM (VISTA Infrared CAMera; Dalton et al. 2006). It has a  $\sim 1 \times 1.5 \text{ deg}^2$  field of view, works in the  $0.9\text{--}2.5 \mu\text{m}$  wavelength range, and has a pixel scale of  $0.34 \text{ arcsec px}^{-1}$ .

The data are reduced with the VISTA Data Flow System (VDFS; Irwin et al. 2004; Emerson et al. 2004) at the Cambridge Astronomical Survey Unit<sup>1</sup> (CASU). Processed images and photometric catalogs are available from the ESO Science Archive<sup>2</sup> and from the VISTA Science Archive<sup>3</sup> (VSA; Cross et al. 2012).

A single VIRCAM image, called pawprint, contains large gaps; six pawprints taken in a spatial offset pattern must be combined to fill them in, obtaining a contiguous image, called tile. Each point of the sky is imaged at least twice within a tile, except of the outermost edges that are imaged once. The VVVX pawprints and tiles are aligned along  $l$  and  $b$ . The total effective exposure time of the tiles are: 8 sec in  $K_S$  (for a single epoch), 24 sec in  $H$  and 60 in  $J$  band.

In order to obtain the best results in such a crowded environment, we extract our own point spread function (PSF) photometry on the different regions of interest. This procedure is described in detail by Alonso-García et al. (2018) and Borissova et al. (2011, 2014) and enhances the depth of CASU aperture photometry, typically by 1-2 mag, along with the completeness of our data. The magnitudes, calibrated in the VISTA system, were transformed to the 2MASS standard system, and the saturated stars (usually with  $K_S \leq 11.5$  mag, depending on crowding) were replaced

<sup>1</sup> <http://casu.ast.cam.ac.uk/>

<sup>2</sup> <http://archive.eso.org/>

<sup>3</sup> <http://horus.roe.ac.uk/vsa/>

with 2MASS photometry, following Alonso-García et al. (2018).

### 3 CLUSTER SEARCH AND CANDIDATE SELECTION

We searched cluster candidates by means of visual inspection, as in our previous works (Borissova et al. 2011, 2014, 2018). The observed images were retrieved from the CASU database. Initially the  $K_S$  tiles were visually inspected, creating a preliminary list of candidates. The main criterion was the presence of a local overdensity with respect to the surrounding area and (or) visually connected with any surrounding nebulousity. Then, composite  $JHK_S$  color images were created. We verified the compact nature of the object and required at least 5-6 stars with similar colors to be clustered at the objects' center. This method was preferred over various automatic algorithms that count stars, in order to include objects that are not fully resolved into members.

We have identified 88 new cluster candidates. They are listed in Table A1. The first column gives the identification, followed by the equatorial coordinates of the center determined by eye, eye-ball measured apparent cluster radius in arcmin, the name of the corresponding VVVX tile, distance to the candidate in kpc (if available), *Herschel* SPIRE 500  $\mu\text{m}$  measured flux in Jy, *WISE* W4 22  $\mu\text{m}$  measured flux in Jy, dust mass in units of solar masses (both variables are described below in the text) and any nearby associated (within the visual cluster diameter) objects such as IR sources, YSOs, H II regions, dense cores, etc. The cluster radii were measured by eye on the VVVX  $K_S$  tiles. To do this, the area around cluster candidates is smoothed and the stellar density contours are over-plotted with the lowest contour corresponding to the stellar density of comparison field.

Figures 2 and 3 show the VVVX  $JHK_S$  color images of some of them for illustration.

### 4 VALIDATION AND PRELIMINARY CLASSIFICATION

#### 4.1 Obscured cluster candidates

According to Ascenso (2018) “An embedded cluster is one that is still enshrouded in its natal molecular cloud. It is typically not (fully) observable at optical wavelengths due to the heavy obscuration caused by the dust grains in the cloud, but it can be seen in the near infrared, where young stars emit significantly and the dust is more transparent”. As pointed out in the same review, the upper limit of the age of such objects is 5-10 Myr.

To investigate the probability of physical connection between our cluster candidates and any remaining dust and gas in their vicinities, we overplot the cluster candidates on far-IR color images. Some good tracers of cold dust are *Herschel* PACS (70  $\mu\text{m}$  – blue, 160  $\mu\text{m}$  – red; Poglitsch et al. 2010) and SPIRE (250  $\mu\text{m}$  – blue; 350  $\mu\text{m}$  – green; and 500  $\mu\text{m}$  – red; Griffin et al. 2010). These are taken from the archival HiGal survey (Molinari, et al. 2010). Fifty four (61 %) of our 88 candidates have *Herschel* data, the rest are projected outside of the field of view. We performed aperture photometry

on the *Herschel* SPIRE 500  $\mu\text{m}$  normalized image, chosen because of the lower mean temperature of the dust (18.7 K, Zhu et al. 2014). The diameter of aperture was determined on the base of flux contours. The typical flux density uncertainty is 15%. The mass of the dust is calculated following the calibration of Paron et al. (2012, see Eqn. 1), assuming that the main contribution of the continuum emission come from the dust. Thirty candidates have SPIRE 500  $\mu\text{m}$  fluxes with the  $3\sigma$  values above the local field and are probably still associated with their cold dust. Most of them coincide with the brightest core of the extended dust emission. They are listed in Table A1 together with their corresponding dust mass.

We also verified the projection of our candidates on the *allWISE* color composite (W4 – red; W2 – green; W1 – blue; Wright et al. 2010) image. Table A1 lists the W4 (22  $\mu\text{m}$ ) band fluxes with the  $3\sigma$  values above the local field. The typical flux density uncertainty is around 10%. Only 20 objects can not be connected with any dust emissions in this band.

Figure 4 shows the *Herschel* and *allWISE* images with some candidates overplotted for illustration.

Thus, the emission clumps in the dust continuum in *Herschel* and *allWISE* suggested that 71 (80 %) of our objects can be classified as obscured, possibly still embedded in their natal dust.

In a search for indicators of youth, such as young stellar objects (YSOs), masers, IR sources and H II regions, we cross-identified the objects in our sample with the SIMBAD astronomical database<sup>4</sup> (Wenger et al. 2000). We found indicators of youth for 63 of our candidates (see Table A1 for comments on individual objects). They can be classified as young, with ages of 5-10 Myr or less.

Radial velocities in the local system of rest (VLSR) are available in the literature for 42 of our candidates. Using the Wenger et al. (2018) tool<sup>5</sup>, we calculated their kinematic distances, taking into account the VLSR uncertainties. The tool uses the Reid et al. (2014) MW rotation curve with updated solar motion parameters and evaluates the errors with 10 000 Monte Carlo realizations. It seems optimal for our small size and young clusters. The results are listed in Table A1 and the normalized histogram distributions of VLSRs, distances and cluster radii are shown in Fig. 5. Most of the candidates are located at distances 2-4 kpc from the Sun and have linear diameters of 0.2-1.4 pc.

#### 4.2 Open cluster candidates

Nine clusters (listed in Table A1 from CL 200 to CL 208) are not projected close to any nebulousity, but show up as clear overdensities with respect to the surrounding field. They are resolved or semi-resolved. Here, the validation process includes the analysis of the CMDs (see Borissova et al. 2018, for more details). Distances from *Gaia* Data Release 2 (*Gaia* DR2; *Gaia* Collaboration et al. 2018) and Bailer-Jones et al. (2018) were considered, when available. However, most objects are sparsely populated and only three of them (CL 204,

<sup>4</sup> <http://simbad.u-strasbg.fr/simbad/>

<sup>5</sup> <https://www.treywenger.com/kd/index.php>



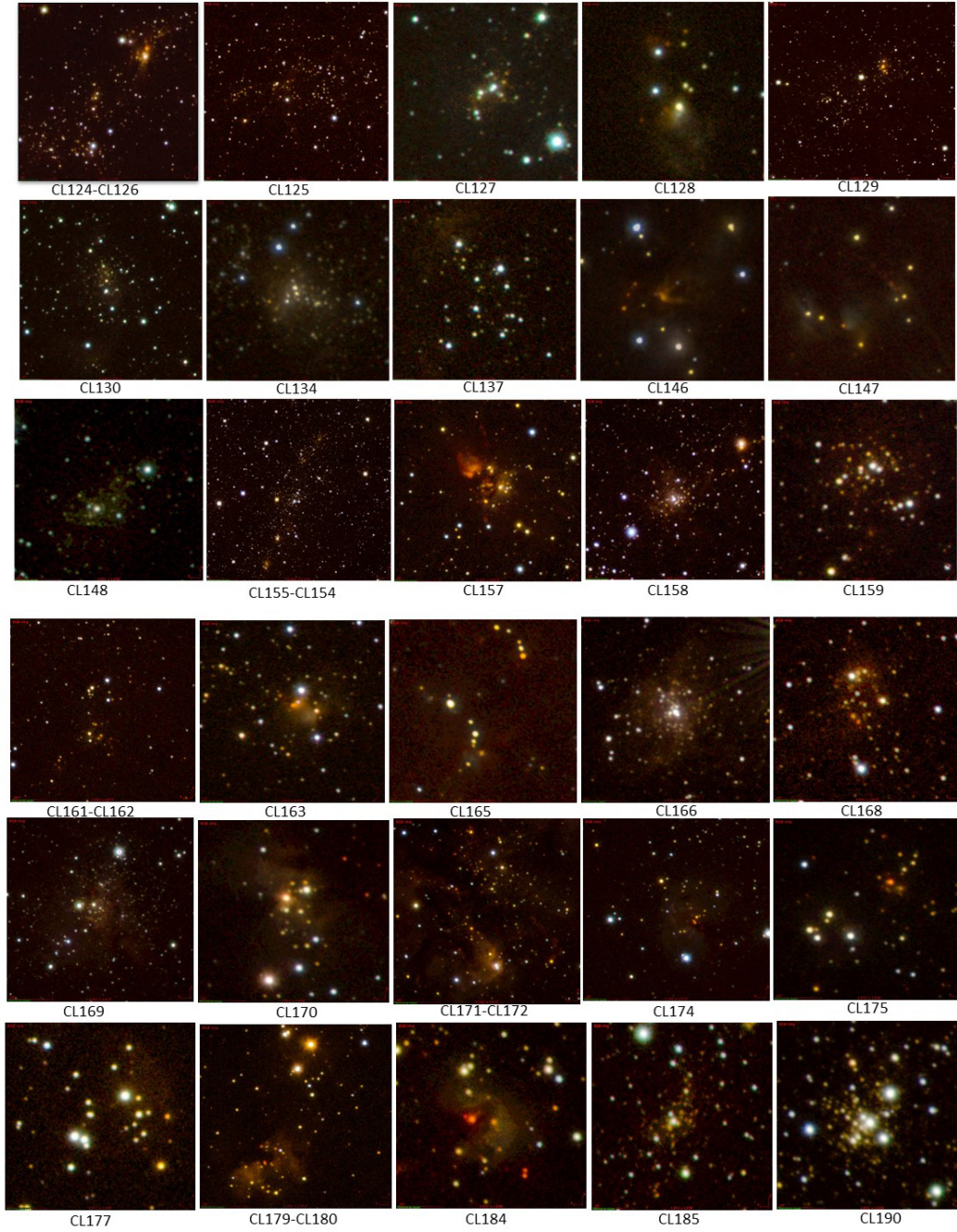


**Figure 2.** VVVX  $JHK_S$  color images for a subset of the newly found cluster candidates. The field of view is typically  $1.5 \times 1.5$  arcmin; North is up, East is to the left.

CL 207 and CL 208) have a high enough number of possible member stars for estimation of any fundamental cluster parameters. Deeper observations with higher angular resolution are needed to reveal the nature of the remaining six open cluster candidates.

For the analysis of VVVX CL 204, CL 207 and CL 208, the first step was to construct their CMDs from the PSF photometry within  $5 \times 5$  arcmin area around the cluster center. Then, the Bonatto (2019) tools  $CLEAN_{phot}$  and  $FitCMD$  were used to decontaminate statistically the CMDs and to perform isochrone fitting, respectively. Importantly, these

tools take into account the photometric errors. The derived parameters are: total stellar mass, cluster age, metallicity, foreground reddening and distance modulus. The clusters CL 207 and CL 208 are moderately reddened (with  $E(J-K_S)$  around 0.55 mag), are relatively close to the Sun (with distance around 3 kpc), and have masses less than  $2000 M_\odot$  and solar metallicity. The cluster CL 204 is an exception. Most probably this object is a dissolving cluster, being the oldest one in the sample (7.5 Gyr), metal poor ( $[Fe/H] = -1.28$  dex.), and with a very small total mass of  $\approx 400 M_\odot$ .

The Hess color magnitude diagrams of the cluster can-

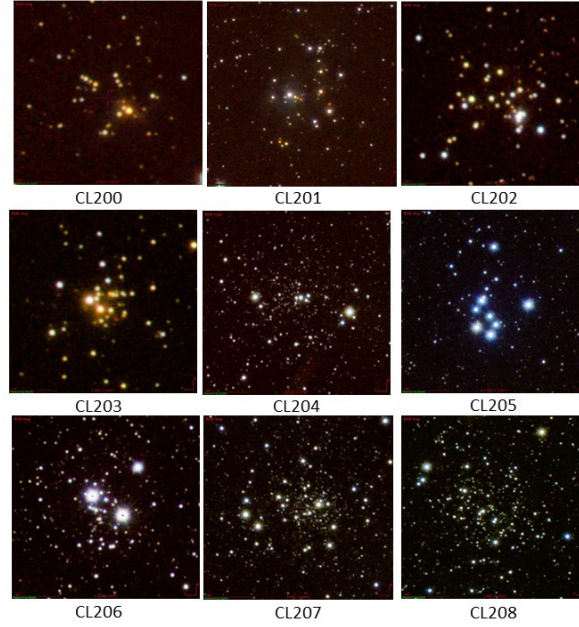


**Figure 3.** VVVX  $JHK_S$  color images of newly found cluster candidates. The field of view is typically 2.5x2.5 arcmin; North is up, East is to the left.

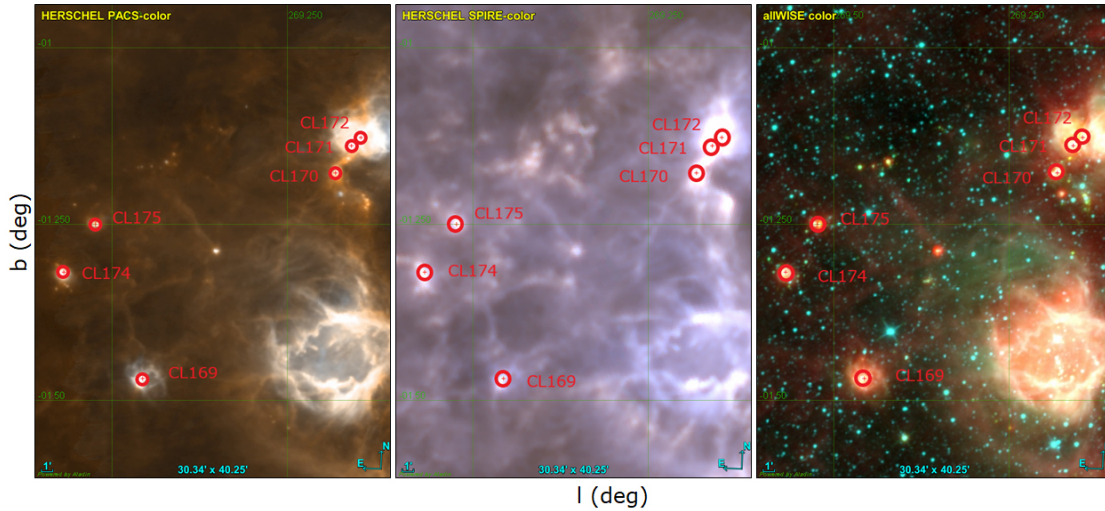


**Figure 4.** *Herschel* PACS and SPIRE and *allWISE* color compositions with overplotted CL 169, 171, 172, 174 and 175. The field of view is 30 x 40 arcmin; the North is up, East is to the left.

didates CL 204, CL 207 and CL 208 are plotted in Fig. 6 and the derived parameters are listed in Table B3.

## 5 KNOWN CLUSTERS IN THE AREA

Bica et al. (2019) summarized the known open clusters or candidates at that time and listed in total about 10 000 objects; 2454 of them fall within the area studied here. From this subset, 817 were classified by the authors as “embedded cluster (EC)”, “embedded cluster candidate (ECC)” or

“embedded group (EGr)”. Our visual search didn’t recover 90 candidates listed in the catalog, mainly from the WISE-based discoveries (Camargo, Bica, & Bonatto 2016). On the VVVX images they typically appear as one or two bright stars or windows in the dust screen. The coordinates and designation names as in Bica et al. (2019) catalog are listed in Table B1.

On the other hand, we confirmed by the same method 71 objects, classified by the authors as embedded clusters and visually connected with the surrounding nebosity in the VVVX images. They are verified also on the *Herschel* and *allWISE* color compositions. Figure 7 shows the dis-



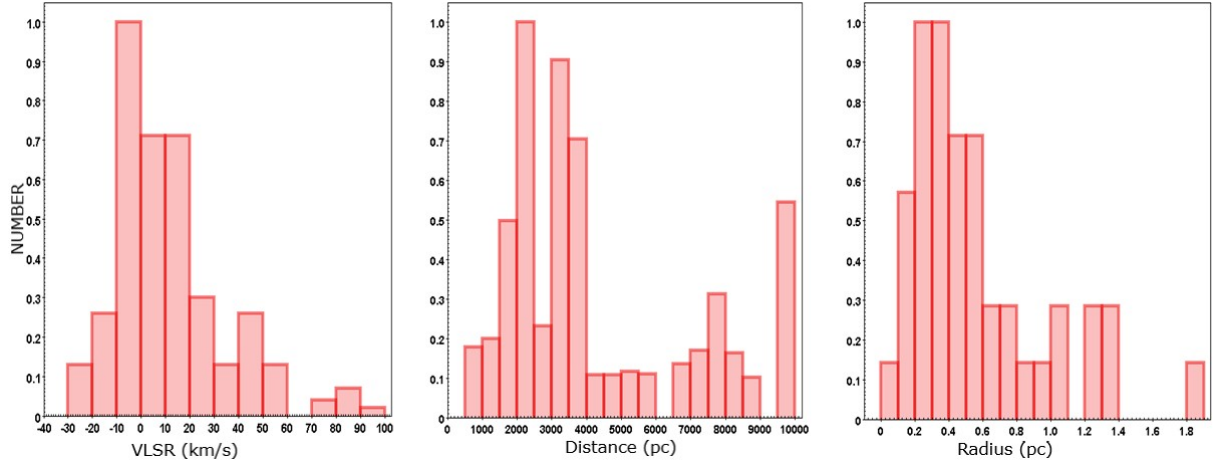


**Figure 5.** Normalized distributions of (left to right): VLSR ( $\text{km s}^{-1}$ ), kinematic distance (pc) and linear radius (pc) of the cluster candidates.

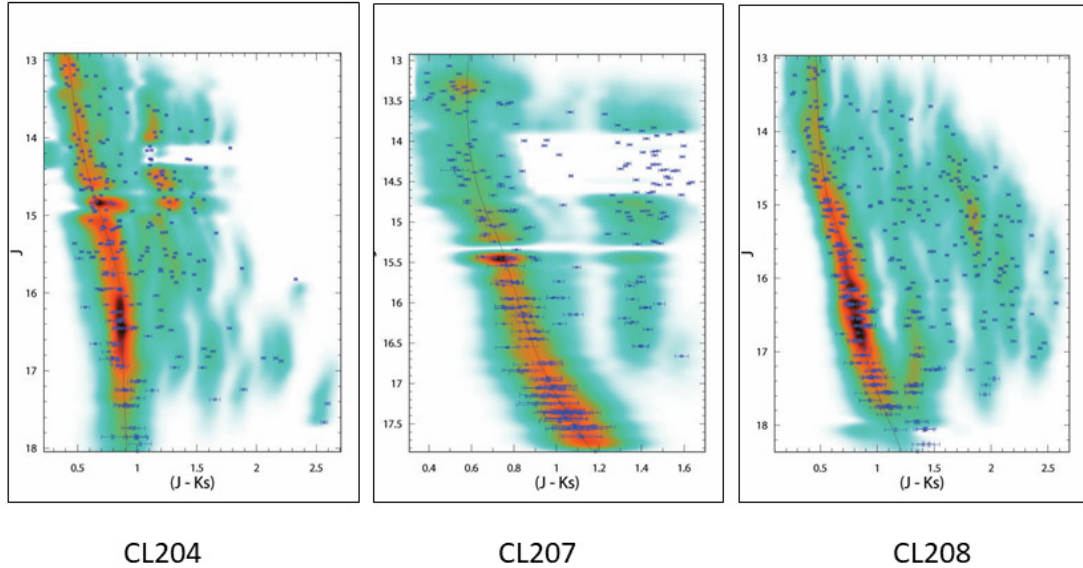


**Figure 6.** Hess color magnitude diagrams of the cluster candidates VVVX CL 204, CL 207 and CL 208.

tribution of Bica’s objects on the *allWISE*, with a zoomed *Herschel* area for illustration. Note, that we also overplotted the candidates proposed in this paper (blue circles). The coordinates and designation names as in Bica et al. (2019) catalog are listed in Table B2.

We chose 15 of Bica’s objects, projected close to our newly discovered candidates or visually on the same nebulosity; with enough resolved member stars and without any determined basic parameters in the literature. Figure 8 shows some examples.

Then we performed color-magnitude analysis, using the same technique as for our open cluster candidates (Sec. 4.2). For the most probable cluster member stars – as identified with *CLEAN<sub>phot</sub>* and *FitCMD* – we also report *Gaia* Data Release 2 distances from Bailer-Jones et al. (2018). For each cluster we adopted an average distance obtained by fitting a Gaussian function to the distribution of the *Gaia* distance

determinations of individual members. We found a good agreement between the astrometric and the *FitCMD*-derived distances, with measured correlation of 92% of the linear fit and some systematic effect of 200 pc, where the *Gaia* distances put the objects closer to the Sun. The derived cluster parameters are listed in Table B3 (alongside the new VVVX clusters), and the CMDs are shown in Fig. B1. The sample contains not very obscured ( $E(J - K)$  between 0.18 and 0.55 mag), low mass (72% have masses below  $2000 M_{\odot}$ ) and relatively young (between 20 and 650 Myr) clusters. Most of the clusters show solar metallicity. The clusters CL 204 and Teu 215 are exceptions, showing higher masses and older ages. In Fig. 9 are shown some relations with the above derived basic cluster parameters. In general, these relations follow the expected distribution for typical open clusters, for example, decreasing  $[\text{Fe}/\text{H}]$  with increasing cluster age. The *Gaia* derived proper motions show that all seem to be

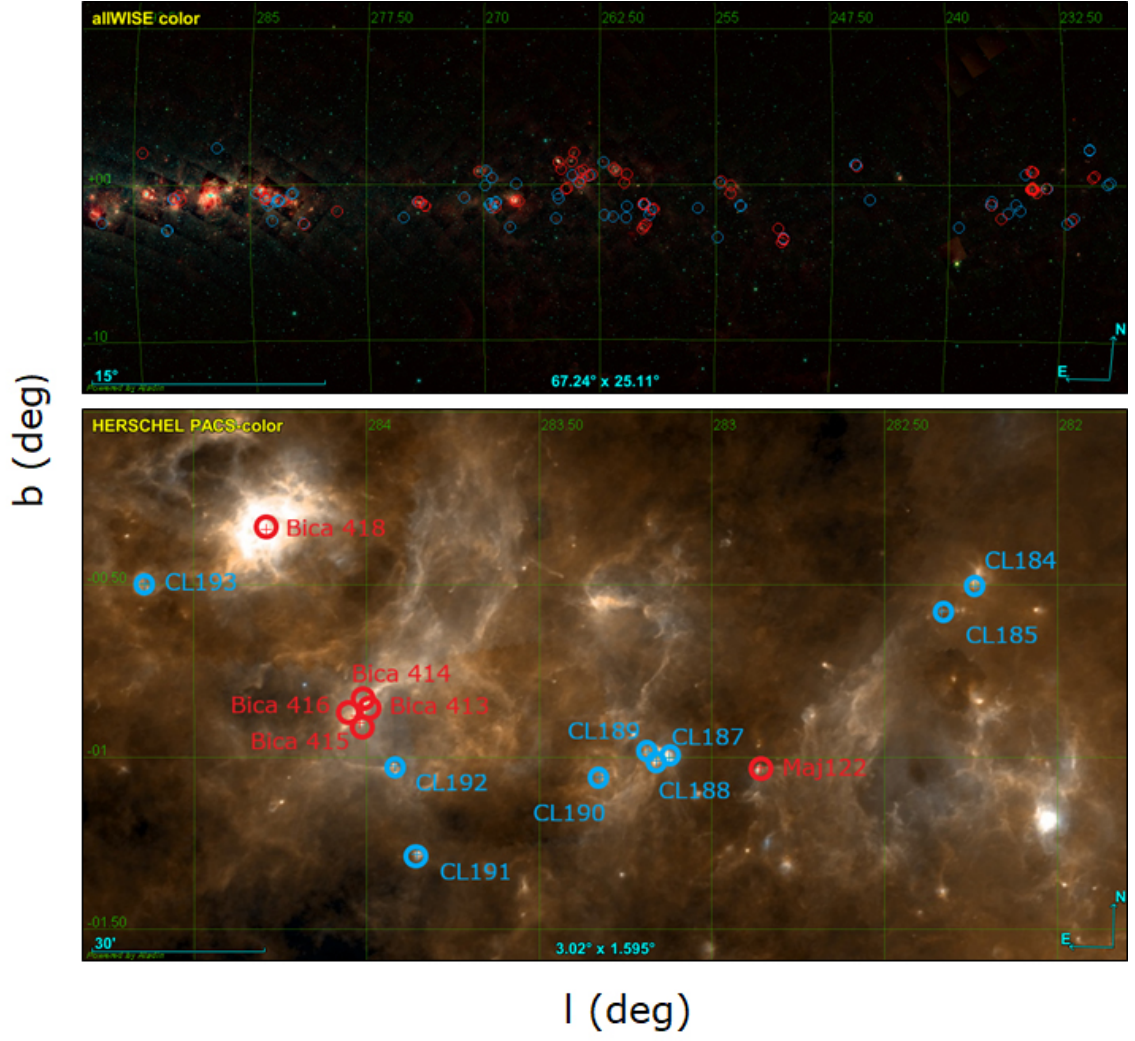


**Figure 7.** The distribution of visually confirmed obscured clusters from Bica et al. (2019) (red circles) and newly proposed in this paper VVVX clusters (blue circles) overplotted on *allWISE* and *Herschel* images.

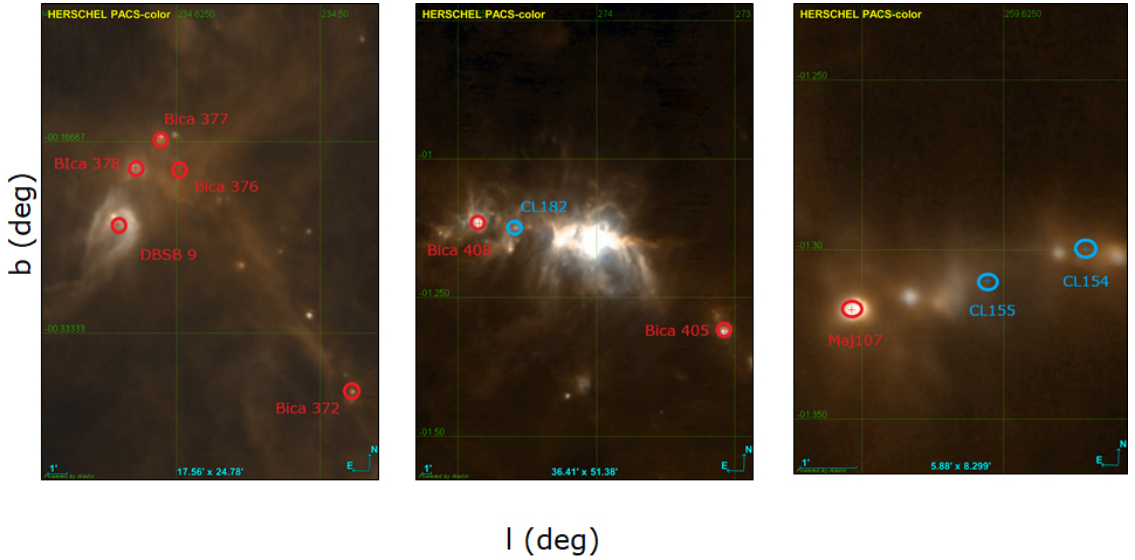


**Figure 8.** *Herschel* PACS (70 $\mu$ m and 160 $\mu$ m) color composition with overplotted group of clusters. North is up, East is to the left.

moving in the same direction, indicating that they belong to the disk population.

The rest of the [Bica et al. \(2019\)](#) clusters, classified by these authors as “embedded” and projected on the investigated area, are known and relatively big young clusters, or cannot be associated with any projected nebulosity in the VVVX images. Their analysis is outside the scope of this paper. We also do not include any of the projected in the area of massive young clusters such as NGC 3603, Westerlund 2 and the Carina Nebula Complex.

## 6 SPATIAL DISTRIBUTION OF THE SAMPLE

Combining all 60 clusters with the above derived distances (42 from Table A1 (regular font) and 18 from Table B3) allows us to look for spatial clustering. Indeed, the visual inspection of the objects identified several groups of clusters.

The group containing Bica 376, Bica 377, Bica 378, BDSB 9, Bica 372 is shown in Fig. 8, left panel. Judging from the network of filaments connecting the dust emission density peaks, as well as similar withing the errors distances, these objects seem to be physically connected and to lie on the same cloud. Another group of clusters is shown in Fig. 4. The mean distance of CL 169, 171, 172, 174 and 175 is determined as  $2.3 \pm 0.3$  kpc, thus most probably they belong to the same cloud. One more cluster candidate, CL 170, is projected in the area, without distance measurements, and we assume the mean distance of the group as the distance to this object. The group Bica 405 and Bica 408 shows mean distance of  $3.4 \pm 0.3$  kpc. We can adopt this value for the cluster CL 182. The group CL 187, 188, 189 has distance of  $3.7 \pm 0.4$  kpc, so this value can be adopted for CL 190. Maj 107 has  $2.9 \pm 0.1$ , so we assume that the clusters CL 154 and 155 are placed on the same distance. We mark the adopted distances in Table A1 with bold font.

## 7 SUMMARY

In the latest observed area of the VVVX survey we report a catalog of 88 new cluster candidates. Radial velocities, available in the literature for 42 of them allow us to determine their kinematic heliocentric distances, placing most of them between 2 and 4 kpc. These are small clusters, with linear diameters between 0.2 and 1.4 pc. Comparison with fluxes of the emission clumps in the dust continuum of *Herschel* and *allWISE* shows that 80 % of them most probably are still associated with their cold dust.

Additionally, nine candidates are proposed to be older open cluster candidates. Three of them have sufficient number of well-resolved stellar members, which allow us to determine some basic cluster parameters. We confirm their nature as older, low-mass open clusters. VVVX CL 204 could be “dissolving” cluster, according to its low total cluster mass, low metallicity and older age.

During our visual inspection of VVVX image we did not recover 90 embedded cluster candidates listed in [Bica et al. \(2019\)](#), and confirmed 71 of them on the base of their appearance on the high quality VVVX images. Photometric analysis of 15 clusters from [Bica et al. \(2019\)](#) catalog shows that they have ages above 20 Myr, masses below  $2000 M_{\odot}$

and in general follow the motion of the disk, according to their proper motion distribution.

The distance determinations allow us to outline some groups of clusters, most probably formed within the same dust complex. When possible, the mean distance value is assigned to nearby projected clusters, without their own measurements. In general, our candidates follow the network of filaments structures of the renaming dust.

Thus, in the this VVVX area, we found recent star formation, which produce small size and young clusters, in addition to the well know, massive young clusters of the MW, including NGC 3603, Westerlund 2 and the Carina Nebula Complex.

## ACKNOWLEDGEMENTS

We gratefully acknowledge data from the ESO Public Survey program ID 198.B-2004 taken with the VISTA telescope, and products from the Cambridge Astronomical Survey Unit (CASU). This work has made use of data from the European Space Agency (ESA) mission *Gaia*<sup>6</sup>, processed by the *Gaia* Data Processing and Analysis Consortium (DPAC)<sup>7</sup>. Funding for the DPAC has been provided by national institutions, in particular the institutions participating in the *Gaia* Multilateral Agreement. Support is provided by the ANID, Millennium Science Initiative, PROG. ICM ANID, ICN12-009, awarded to the Millennium Institute of Astrophysics (MAS). J.A.-G. also acknowledges support from Fondecyt Regular 1201490. S.R.A. acknowledges support from the FONDECYT Iniciación project 11171025, the FONDECYT Regular project 1201490, and the CONICYT + PAI “Concurso Nacional Inserción de Capital Humano Avanzado en la Academia 2017” project PAI 79170089. This research has made use of the SIMBAD database, operated at CDS, Strasbourg, France. We are grateful to the referee Dr. Joana Ascenso for very useful comments, which greatly improve the manuscript.

Data availability: The data underlying this article are available in the article and in its online supplementary material.

<sup>6</sup> <https://www.cosmos.esa.int/gaia>

<sup>7</sup> <https://www.cosmos.esa.int/web/gaia/dpac/consortium>



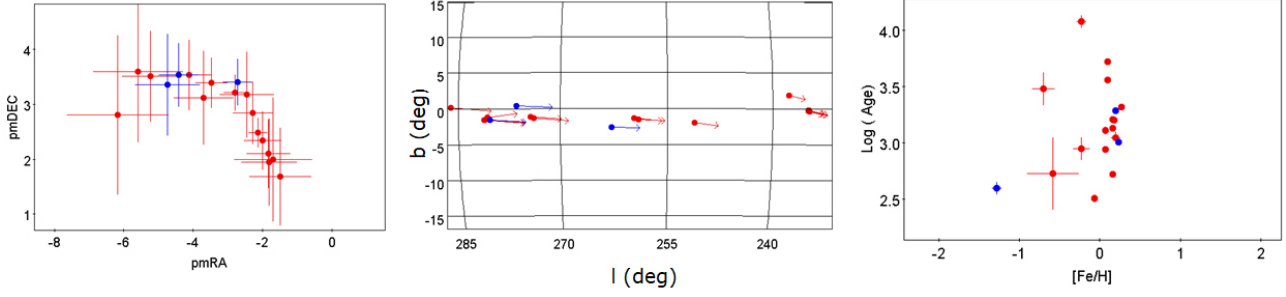


**Figure 9.** Parameters of the open cluster sample. The blue color stands for the newly proposed candidates.

## REFERENCES

- Ascenso, J. 2018, *Astrophysics and Space Science Library*, Volume 424, 1A
- Alonso-García J., Saito, R. K., Hempel, M., et al., 2018, *A&A*, 619, A4
- Bailer-Jones, C. A. L., Rybizki, J., Foesneanu, M., Mantelet, G. et al. 2018, *AJ*, 156, 58B
- Bonatto, Charles 2019, *MNRAS*, 483,2758B
- Barbá, R. H., Roman-Lopes, A., Nilo Castellón, J. L., et al. 2015, *A&A*, 581, A120
- Benjamin, R. A., Churchwell, E., Babler, B. L., et al. 2003, *PASP*, 115, 953
- Bica, E., Dutra, C. M., Soares, J., et al. 2003, *A&A*, 404, 223
- Bica, E., Pavani, D. B., Bonatto, C. J., Lima, E. F. 2019, *AJ*, 157, 12B
- Borissova, J., Bonatto, C., Kurtev, R., et al. 2011, *A&A*, 532, A131
- Borissova, J., Chené, A.-N., Ramírez Alegría, S., et al. 2014, *A&A*, 569, A24
- Borissova, J., Ivanov, V. D., Lucas, P. W., et al. 2018, *MNRAS*, 481, 3902
- Camargo D., Bica E., Bonatto C., 2016, *MNRAS*, 455, 3126C
- Cantat-Gaudin, T., Jordi, C., Vallenari, A., et al. 2018, *A&A*, 618, A93
- Cantat-Gaudin, T., Krone-Martins, A., Sedaghat, N., et al. 2019, *A&A*, 624, A126
- Cantat-Gaudin, T., & Anders, F. 2020, *A&A*, 633, A99
- Cross, N. J. G., Collins, R. S., Mann, R. G., et al. 2012, *A&A*, 548, A119
- Dalton, G. B., Caldwell, M., Ward, A. K., et al. 2006, in *SPIE Conf. Ser.*, 6269, 30
- Dutra, C. M., Bica, E., Soares, J., et al. 2003, *A&A*, 400, 533
- Emerson, J., McPherson, A., & Sutherland, W. 2006, *The Messenger*, 126, 41
- Emerson, J. P., Irwin, M. J., Lewis, J., et al. 2004, in *SPIE Conf. Ser.*, 5493, 401
- Froeblich, D., Scholz, A., & Raftery, C. L. 2007, *MNRAS*, 374, 399
- Gaia Collaboration, Prusti, T., de Bruijne, J. H. J., et al. 2016, *A&A*, 595, A1
- Gaia Collaboration, Brown, A. G. A., Vallenari, A., et al. 2018, *ArXiv e-prints*, arXiv:1804.09365
- Gaia Collaboration, Helmi, A., van Leeuwen, F., et al. 2018, *arXiv:1804.09381*
- Gran F., Zoccali M., Contreras Ramos R., Valenti E., Rojas-Arriagada A., Carballo-Bello J. A., Alonso-Garcia J., et al., 2019, *A&A*, 628, A45
- Griffin, M. J., Abergel, A., Abreu, A. et al. 2010 *A&A*, 518L, 3G
- Irwin, M. J., Lewis, J., Hodgkin, S., et al. 2004, in *SPIE Conf. Ser.*, 5493, 411
- Ivanov, V. D., Piatti, A. E., Beamín, J.-C., et al. 2017, *A&A*, 600, A112
- Lindegren, L., Hernandez, J., Bombrun, A., et al. 2018, *arXiv:1804.09366*
- LSST Science Collaboration. 2009, *ArXiv e-prints*, arXiv:0912.0201
- Luri X., et al., 2018, *A&A in press*, arXiv, arXiv:1804.09376
- Minniti, D., Lucas, P.W., Emerson, J.P., et al. 2010, *NewA*, 15, 433
- Moitinho, A. 2010, *Star Clusters: Basic Galactic Building Blocks Throughout Time and Space*, 106
- Molinari S., et al., 2010, *PASP*, 122, 314
- Paron, S., Combi, J. A., Petriella, A., Giacani, E. 2012, *A&A*, 543, A23
- Poglitsch, A., Waelkens, C., Geis, N. et al. 2010 *A&A*, 518L, 2P
- PACS
- Reid, M. J., Menten, K. M., Brunthaler, A., Zheng, X. W. et al. 2014, *ApJ*, 783, 130R
- Saito, R.K., Hempel, M., Minniti, D., et al. 2012, *A&A*, 537, 107
- Schmeja, S., Kharchenko, N.V., Piskunov, A.E., et al. 2014, *A&A*, 568, 51
- Skrutskie, M.F., Cutri, R.M., Stiening, R., et al. 2006, *AJ*, 131, 1163
- Solin, O., Haikala, L., & Ukkonen, E. 2014, *A&A*, 562, A115
- Stanghellini, L., Shaw, R. A., & Villaver, E. 2008, *ApJ*, 689, 194
- Wright, E.L., Eisenhardt, P.R.M., Mainzer, A.K., et al. 2010, *AJ*, 140, 1868
- Wenger, Trey V., Balser, D.S., Anderson, L. D., Bania, T. M. 2018, *AJ*, 856, 52
- Wenger, M., Ochsenbein, F., Egret, D., et al. 2000, *A&AS*, 143, 9
- Zhu, Jiali and Huang, Maohai 2014, *A&A* 564, A111

## APPENDIX A: THE CATALOG OF NEWLY DISCOVERED VVVX CLUSTER CANDIDATES.

In Table A1 are tabulated the newly proposed candidate star clusters. The first column gives the identification, followed by the equatorial coordinates of the center, eye-ball measured apparent cluster radius in arcmin, the name of the corresponding VVVX tile, distance to the candidate in kpc, *Herschel* SPIRE 500 $\mu$ m and WISE W4 (22 $\mu$ m) flux in Jy, calculated mass of the dust in solar masses and any known nearby objects such as IR sources, YSOs, H II regions, dense cores (when available), taken from the SIMBAD database (<http://simbad.u-strasbg.fr/simbad/>).

## APPENDIX B: KNOWN CLUSTERS IN THE REGION.

**Table A1.** Catalog of newly proposed VVVX clusters.

Name	$\alpha\delta(J2000)$ °	Radius arcmin	VVVX tile	Kinem. Dist. kpc	F500 $\mu$ m Jy	F22 $\mu$ m Jy	M <sub>dust</sub> M <sub>⊙</sub>	Comments
VVVX CL121	109.7116 −18.3699	0.42	e686			283		IRAS 07166-1816 – Far-IR source
VVVX CL122	109.7168 −18.3805	0.42	e686					no known sources
VVVX CL123	109.7930 −17.8238	0.25	e685			358		MSX6C G231.9005-02.1378 – HII (ionized) region
VVVX CL124	110.7560 −14.6912	0.60	e1091	3.2±1.0	264	387	386	[BNM96] 229.570+0.150 – HII (ionized) region
VVVX CL125	110.7717 −14.9151	0.83	e1091			163		no known sources
VVVX CL126	110.7734 −14.7108	0.92	e1091			173		no known sources
VVVX CL127	111.9843 −20.6689	0.47	e1005	7.4±1.3	171	269	1347	IRAS 07257-2033 – Far-IR source
VVVX CL128	112.2242 −21.4514	0.10	e1005	2.3±0.6	253	190	183	IRAS 07267-2120 – Far-IR source
VVVX CL129	112.4938 −18.4728	1.48	e1048					no known sources
VVVX CL130	112.5211 −20.7384	0.65	e1005	6.7±1.1	215	279	1360	BRAN 33A – Star forming region
VVVX CL131	112.9961 −24.6527	0.42	e690			211		PN G239.3-02.7 – Possible Planetary Nebula
VVVX CL132	113.0043 −24.6423	0.33	e690			170		no known sources
VVVX CL133	113.3238 −14.8495	0.42	e768			184		no known sources
VVVX CL134	113.3329 −22.1824	0.43	e1006			471		BRAN 45 – Interstellar matter
VVVX CL135	113.3457 −14.8520	0.58	e768			169		no known sources
VVVX CL136	113.3731 −14.8568	0.67	e768			181		no known sources
VVVX CL137	113.4895 −22.0031	0.43	e1006	1.7±0.7	200	194	82	BRAN 47 – HII (ionized) region
VVVX CL138	113.9709 −19.2728	0.97	e1094	3.5±0.8		190		IRAS 07336-1909 – HII (ionized) region
VVVX CL139	117.8957 −28.7996	0.35	e1056	7.9±1.4	141		1244	IRAS 07495-2840 – Far-IR source
VVVX CL140	118.5640 −35.0801	0.33	e615			163		no known sources
VVVX CL141	118.5682 −35.0694	0.27	e615			170		IRAS 07523-3456 – Far-IR source
VVVX CL142	118.7334 −34.8285	0.58	e615			340		VLA G250.6504-03.4733 – HII (ionized) region
VVVX CL143	120.6256 −28.3981	0.40	e1147	4.8±0.9		200		BRAN 98 – Interstellar matter
VVVX CL144	120.6895 −28.4340	0.37	e1147			345		G246.0702+01.2909 1 – YSO Cand.
VVVX CL145	121.5830 −38.4280	0.50	e618	9.6±1.5		214		IRAS 08045-3816 – Far-IR source
VVVX CL146	122.6767 −36.0521	0.78	e1017	1.1±0.7	293	432	54	IRAS 08088-3554 – HII (ionized) region
VVVX CL147	122.7522 −36.0806	0.75	e1017			371		2MASX J08110108-3605007 – IR source
VVVX CL148	124.4691 −38.4564	0.75	e1019	8.4±1.3	153	186	1534	IRAS 08160-3818 – Far-IR source
VVVX CL149	125.1917 −36.3529	0.32	e1108			248		IRAS 08188-3611 – Far-IR source
VVVX CL150	125.7669 −41.9324	0.20	e704			438		2MASX J08230395-4155551 – YSO Candidate
VVVX CL151	126.3285 −41.2428	0.13	e1021	5.6±0.9	126	221	572	IRAS 08235-4104 – Far-IR source
VVVX CL152	126.5715 −40.8113	0.23	e1021	1.8±0.7	203	440	98	[MHL2007] G259.0453-01.5559 1 – YSO Cand.
VVVX CL153	126.6394 −41.0106	0.25	e1021	2.0±1.3	162	258	93	IRAS 08247-4050 – Far-IR source
VVVX CL154	127.2737 −41.1136	0.77	e1021	<b>2.9±0.1</b>		181		no known sources
VVVX CL155	127.2863 −41.1424	0.47	e1021	<b>2.9±0.1</b>				no known sources
VVVX CL156	127.3320 −42.5772	0.27	e1022			191		no known sources
VVVX CL157	128.0324 −43.2308	0.93	e1023	2.2±0.8	217	478	149	IRAS 08303-4303 – HII (ionized) region
VVVX CL158	128.0538 −42.0740	0.35	e1022	2.1±0.8	150	205	97	IRAS 08304-4153 – Far-IR source
VVVX CL159	128.6130 −43.5796	0.45	e1023	1.9±0.9	172	189	85	IRAS 08327-4324 – Far-IR source
VVVX CL160	131.0680 −46.1999	0.33	e708	5.1±0.9	158	286	595	IRAS 08426-4601 – HII (ionized) region
VVVX CL161	132.1944 −42.7424	0.25	e1114					no known sources
VVVX CL162	132.1958 −42.7510	0.17	e1114					no known sources
VVVX CL163	132.2759 −45.2612	0.42	e1070	3.6±0.8	163	318	309	IRAS 08473-4504 – HII (ionized) region
VVVX CL164	132.3000 −41.5764	0.45	e1158	1.0±1.4		230		ESO-HA 196 – Emission-line Star
VVVX CL165	132.3061 −43.6065	0.48	e1114	9.7±2.8	202	203	2724	2MASS J08491394-4336092 – YSO
VVVX CL166	132.6621 −45.1388	0.42	e1070	1.6±0.8	185		69	TGU H1699 – Dark Cloud (nebula)
VVVX CL167	133.1393 −48.8477	0.25	e710			178		IRAS 08509-4839 – Far-IR source
VVVX CL168	133.1728 −43.6181	0.60	e1114	1.4±0.8				IRAS 08509-4325 – Dense core
VVVX CL169	135.8099 −48.9216	0.85	e1028	2.2±0.9	243	503	172	IRAS 09015-4843 – HII (ionized) region
VVVX CL170	135.8627 −48.5216	0.60	e1028	<b>2.3±0.3</b>		351		IRAS 09017-4819 – IR source
VVVX CL171	135.8838 −48.4790	0.47	e1073	2.5±1.0	395	1019	358	IRAS 09018-4816 – HII (ionized) region
VVVX CL172	135.8840 −48.4616	0.65	e1073	2.7±0.8	395	664	411	[HBM2005] G269.15-1.13 – mm radiosource
VVVX CL173	135.8992 −46.7214	0.28	e1117	2.2±0.9	240	171	166	IRAS 09018-4631 – HII (ionized) region
VVVX CL174	136.0951 −48.9045	0.68	e1028	2.2±0.8	249	349	169	IRAS 09026-4842 – Far-IR source
VVVX CL175	136.1257 −48.8259	0.62	e1028	2.0±0.9	254	342	150	IRAS 09028-4837 – HII (ionized) region
VVVX CL176	137.7850 −48.2656	0.42	e1073			488		[BNM96] 269.854-0.063 – HII (ionized) reg.
VVVX CL177	137.8902 −47.6336	1.35	e1118	1.9±0.8		220		IRAS 09098-4725 – Far-IR source
VVVX CL178	138.3333 −49.7635	0.60	e1074			172		IRAS 09116-4933 – Far-IR source
VVVX CL179	138.7102 −47.5774	0.82	e1118			279		no known sources
VVVX CL180	138.7209 −47.6009	0.60	e1118	2.2±0.9		441		IRAS 09131-4723 – Far-IR source

**Table A1** – *continued* Catalog of newly proposed VVVX clusters.

Name	$\alpha\delta(J2000)$ °	Radius arcmin	VVVX tile	Kinem. Dist. kpc	F500 $\mu$ m Jy	F22 $\mu$ m Jy	M <sub>dust</sub> M <sub>☉</sub>	Comments
VVVX CL181	141.2859 –53.4727	0.28	e1032	7.7±1.0	135	226	1135	IRAS 09235-5315 – Far-IR source
VVVX CL182	141.2958 –52.0718	0.18	e1031	<b>3.4±0.3</b>		261		no known sources
VVVX CL183	149.5112 –57.9644	0.67	e719	3.1±0.7		464		IRAS 09563-5743 – HII (ionized) region
VVVX CL184	152.6955 –56.7787	0.38	e1082	3.7±0.9	277	227	536	[BYF2011] 23a – Dense core
VVVX CL185	152.7636 –56.8935	0.38	e1082			183		IRAS 10092-5638 – Far-IR source
VVVX CL186	152.8120 –58.9722	0.67	e721	3.9±0.6		373		[BYF2011] 38 – Molecular Cloud
VVVX CL187	153.5177 –57.6919	0.90	e1082	3.8±0.7	271	549	560	[BYF2011] 36c – Dense core
VVVX CL188	153.5682 –57.7203	0.50	e1082	3.4±0.9	239	329	382	[BYF2011] 36d – Dense core
VVVX CL189	153.6358 –57.7125	0.28	e1082	3.8±0.7	245	274	493	[BYF2011] 36a – Dense core
VVVX CL190	153.7691 –57.8498	0.38	e1082	<b>3.7±0.4</b>		420		GAL 283.33-01.05 – HII (ionized) region
VVVX CL191	154.3684 –58.3307	0.50	e1038			317		IRAS 10156-5804 – Far-IR source
VVVX CL192	154.7375 –58.1542	0.40	e1084			312		AGAL G283.916-01.024 – sub-mm source
VVVX CL193	156.4277 –58.0976	0.73	e1083					AGAL G284.631-00.511 – sub-mm source
VVVX CL194	163.0621 –56.7763	0.33	e806	3.7±0.9				IRAS 10501-5630 – HII (ionized) region
VVVX CL195	164.3552 –62.8852	0.33	e725	3.3±4.4		308		IRAS 10554-6237 – possible Herbig Ae/Be
VVVX CL196	164.3915 –62.9814	0.30	e725	4.3±0.9		447		IRAS 10555-6242 – HII (ionized) region
VVVX CL197	165.2948 –60.9496	0.48	e1091	8.8±0.8	325	578	3575	IRAS 10591-6040 – Composite object
VVVX CL198	165.4324 –60.9586	0.80	e1091			462		IRAS 10597-6041 – Far-IR source
VVVX CL199	173.6373 –63.9679	0.33	e728			335		IRAS 11322-6341 – YSO Candidate
VVVX CL200	109.8646 –17.8712	0.42	e685					no known sources
VVVX CL201	111.8978 –23.0899	1.00	e689					no known sources
VVVX CL202	121.6348 –37.5006	0.55	e700					no known sources
VVVX CL203	124.1511 –36.2379	0.30	e1062					no known sources
VVVX CL204	128.4525 –44.4484	0.75	e706					no known sources
VVVX CL205	134.4359 –43.1951	0.58	e1160					no known sources
VVVX CL206	137.4686 –48.8665	0.83	e1073					GSC 08173-00182 – OB+?
VVVX CL207	145.6299 –52.4305	1.25	e1123					no known sources
VVVX CL208	148.5833 –56.4236	1.00	e1035					no known sources

This paper has been typeset from a  $\text{\LaTeX}$  file prepared by the author.



**Table B1.** False positive objects from [Bica et al. \(2019\)](#) catalog as revealed by VVVX. The first column gives the sequence number in this table, followed by the identification and galactic coordinates of the center taken from Bica et al.

Seq. Numb.	Name	GLON deg	GLAT deg	Seq. Numb.	Name	GLON deg	GLAT deg	Seq. Numb.	Name	GLON deg	GLAT deg
1	Bica 370	234.32	-0.45	31	Cmg 989	236.98	-2.69	61	Cmg 378	279.12	-1.22
2	Cmg 264	264.54	0.61	32	Bica 410	283.11	-0.97	62	Cmg 379	279.12	-1.22
3	Cmg 266	264.97	0.26	33	Bica 411	283.43	-0.99	63	Cmg 381	279.42	-0.96
4	Cmg 339	275.72	-2.23	34	Bica 412	283.58	-0.97	64	Cmg 382	279.43	-1.69
5	Cmg 340	275.80	-2.2	35	Cmg 1032	239.65	-2.08	65	Cmg 383	279.5	-1.52
6	Cmg 341	275.88	-2.15	36	Cmg 1070	249.96	-3.49	66	Cmg 384	279.52	-1.73
7	Cmg 342	275.97	-2.03	37	Cmg 1073	250.13	-2.97	67	Cmg 385	279.57	-1.42
8	Bica 393	262.26	1.45	38	Cmg 1086	252.08	-4.24	68	Cmg 386	279.67	-1.02
9	Cmg 240	260.81	0.19	39	Cmg 221	259.09	-1.78	69	Cmg 387	279.93	-0.4
10	Cmg 244	261.04	1.03	40	Cmg 225	259.31	-1.62	70	Cmg 388	280.00	-1.2
11	Cmg 260	262.45	-3.06	41	Cmg 228	259.57	-1.44	71	Cmg 389	280.02	-1.42
12	Cmg 269	265.82	0.92	42	Cmg 229	259.64	-1.31	72	Cmg 390	280.37	-1.68
13	Cmg 270	265.84	1.1	43	Cmg 232	259.77	-2.78	73	Cmg 392	280.43	-1.74
14	Maj 106	259.02	-1.91	44	Cmg 236	259.91	-1.33	74	Reyle-Robin 1	269.27	-1.53
15	Cmg 1070	250.01	-3.34	45	Cmg 237	260.08	-1.38	75	BH 23	254.09	-0.97
16	Cmg 222	259.12	-1.74	46	Cmg 242	260.95	0.87	76	Bica 380	234.84	-0.12
17	Cmg 1087	252.58	-4.01	47	Cmg 257	261.78	-3.04	77	Cmg 334	275.14	-1.07
18	Cmg 268	265.68	1.07	48	Cmg 267	265.51	1.34	78	Cmg 253	261.56	-2.51
19	Alessi 43	262.64	1.38	49	Cmg 289	268.62	0.45	79	Cmg 417	281.56	-2.48
20	Cmg 1038	240.75	-1.62	50	Cmg 290	268.65	0.18	80	Cmg 420	281.65	-2.07
21	Cmg 377	279.04	-1.13	51	Cmg 292	269.61	0.94	81	Cmg 421	281.69	-2.06
22	Cmg 393	280.44	-1.83	52	Cmg 293	269.67	1.07	82	Cmg 1075	250.57	-3.43
23	Cmg 988	236.79	-2.25	53	Cmg 295	269.87	0.78	83	Cmg 336	275.57	-2.2
24	Cmg 231	259.73	-1.32	54	Cmg 297	269.97	0.84	84	Cmg 419	281.64	-2.54
25	Cmg 252	261.54	-2.32	55	Cmg 298	270.04	0.76	85	Cmg 380	279.4	-1.68
26	Cmg 1017	238.88	-2.13	56	Cmg 300	270.25	-1.26	86	DBSB 29	264.99	0.99
27	Cmg 993	237.22	-2.9	57	Cmg 315	270.88	-0.72	87	Bica 396	263.5	0.93
28	Cmg 992	237.21	-2.52	58	Cmg 318	270.96	-1.11	88	MLG 11	263.74	0.82
29	Cmg 1081	250.98	-3.1	59	Cmg 332	275.07	-1.09	89	Cmg 255	261.59	-2.47
30	Cmg 985	236.59	-2.3	60	Cmg 359	277.23	0.64	90	HD 77343 Group	265.46	1.46

**Table B2.** Visually confirmed 71 objects from Bica et al. (2019) catalog as revealed by VVVX. The first column gives the sequence number in this table, followed by the identification, equatorial coordinates of the center and assigned classification taken from Bica et al.; the name of the corresponding VVVX tile and the *Herschel* SPIRE 500  $\mu\text{m}$  flux in Jy.

Seq. Numb.	Name	RA deg	DEC deg	Class	Tile	Flux 500 $\mu\text{m}$ Jy	Seq. Numb.	Name	RA deg	DEC deg	Class	Tile	Flux 500 $\mu\text{m}$ Jy
1	Bica 366	109.7484	-18.0493	EC	e1091	260.56 $\pm$ 0.56	37	Bica 391	131.0482	-41.2728	EC	e1114	
2	Bica 356	111.6487	-15.5345	EC	e1091		38	Bica 392	131.3454	-41.2487	EC	e1158	
3	Bica 355	111.6723	-15.4085	EC	e1091		39	Bica 394	132.1325	-42.5997	EC	e1114	
4	Cmg 986	112.1574	-21.9610	EC	e688	264.43 $\pm$ 0.13	41	MLG 10	132.1936	-43.5426	EC	e1114	288.29 $\pm$ 0.51
5	Mayer 3	112.5197	-18.5308	EC	e1048		41	DBSB 23	132.1952	-42.9101	EC	e1159	
6	Bica 371	112.5686	-19.1779	EC	e1049	277.53 $\pm$ 0.35	42	MLG 8	132.3667	-43.2854	EC	e1114	268.90 $\pm$ 0.61
7	Bica 373	112.7852	-19.2598	EC	e1049	276.19 $\pm$ 0.53	43	MLG 17	132.5622	-44.4364	EC	e1070	338.27 $\pm$ 0.09
8	Bica 374	112.8622	-19.2883	EC	e1049	313.84 $\pm$ 0.46	44	MLG 18	132.5920	-44.5096	EC	e1070	267.77 $\pm$ 0.37
9	Bica 375	112.9188	-19.2817	EC	e1049	318.16 $\pm$ 0.22	45	Bica 396	132.8547	-42.8372	EC	e1114	
10	DBSB 9	112.9462	-19.3702	EC	e1049	295.70 $\pm$ 0.14	46	MLG 11	132.9479	-43.0922	EC	e1114	
11	Bochum 6	112.9499	-19.4596	EC	e1049	217.26 $\pm$ 0.44	47	DBSB 28	134.1138	-43.0951	EC	e1159	266.78 $\pm$ 0.37
12	Bica 376	112.9620	-19.2936	EC	e1049	351.10 $\pm$ 0.18	48	DBSB 29	134.2371	-43.9390	EC	e1115	187.61 $\pm$ 0.33
13	Bica 378	112.9824	-19.3286	EC	e1049	322.88 $\pm$ 0.20	49	DB 94	134.5235	-47.3651	EC	e1027	238.40 $\pm$ 0.23
14	Bica 377	113.0000	-19.2966	EC	e1049	315.08 $\pm$ 0.39	50	MLG 14	134.5506	-42.6234	EC	e1159	316.05 $\pm$ 0.38
15	Maj 91	113.3036	-22.1316	EC	e1006	243.41 $\pm$ 0.09	51	RCW 38	134.7503	-47.4968	EC	e1027	395.68 $\pm$ 0.07
16	DBSB 7	113.8947	-18.7598	EC	e1094		52	RCW 3	134.8560	-43.7523	EC	e1160	338.27 $\pm$ 0.09
17	DBSB 8	113.9163	-18.8170	EC	e1094		53	Gum 25	135.5417	-48.7083	EC	e1028	276.98 $\pm$ 0.06
18	Bica 379	114.0365	-18.8567	EC	e1094		54	DBSB 36	139.1830	-47.9367	EC	e1118	
19	Cmg 1077	118.5627	-35.0735	EGr	e615		55	Bica 405	140.5117	-51.9436	EC	e1031	202.82 $\pm$ 0.44
20	YEP 1	118.6574	-34.9108	EC	e615		56	Bica 406	140.6493	-51.9432	EC	e1031	223.25 $\pm$ 0.38
21	Cmg 1076	118.6574	-34.9108	EC	e615		57	DBSB 38	141.0975	-51.9904	EC	e1031	373.95 $\pm$ 0.28
22	Slotegraaf 14	118.6951	-34.8458	EC	e615		58	Bica 407	141.1785	-52.0252	EC	e1031	357.85 $\pm$ 1.07
23	Magakian 303	119.6409	-34.7959	EC	e698		59	Bica 408	141.3874	-52.1083	EC	e1031	242.74 $\pm$ 0.30
24	Bica 385	120.4785	-28.3832	EC	e1147		60	Cmg 380	147.3309	-55.9953	EC	e1035	202.88 $\pm$ 0.15
25	DBSB 16	123.9972	-36.1438	EC	e1062	305.60 $\pm$ 0.30	61	Cmg 415	149.3425	-57.9856	EC	e0719	193.96 $\pm$ 0.34
26	Maj 95	124.4788	-35.8808	EC	e1062	284.59 $\pm$ 0.84	62	Maj 122	153.0845	-57.5643	EC	e1082	217.55 $\pm$ 0.49
27	Collinder 182	125.2111	-36.2147	EC	e1108	177.97 $\pm$ 0.10	63	Bica 415	155.0290	-58.1034	EC	e1083	
28	DBSB 18	125.7159	-42.1341	EC	e704		64	Bica 413	155.0545	-58.0644	EC	e1083	
29	Maj 103	125.7555	-41.9311	EC	e704		65	Bica 414	155.0648	-58.0561	EC	e1083	
30	Maj 104	125.8144	-41.7666	EC	e704		66	Bica 416	155.0656	-58.0921	EC	e1083	
31	Cmg 219	126.5274	-40.8767	EC	e1021	171.87 $\pm$ 0.05	67	Bica 418	156.0267	-57.7777	EC	e1083	269.22 $\pm$ 0.15
32	Cmg 218	126.5799	-40.8117	EC	e1021	211.83 $\pm$ 0.21	68	Maj 131	164.4179	-60.7654	EC	e1087	223.53 $\pm$ 0.09
33	Maj 107	127.3060	-41.1815	EC	e1021	134.89 $\pm$ 0.09	69	Maj 134	164.8180	-60.5807	EC	e1087	236.91 $\pm$ 0.19
34	Cmg 230	127.3910	-41.1846	EC	e1021	127.68 $\pm$ 0.32	70	Maj 137	165.2671	-60.8460	EC	e1087	317.81 $\pm$ 0.20
35	MLG 3	129.8329	-41.3375	EC	e1112	233.77 $\pm$ 0.21	71	DBSB 64	171.1679	-58.9359	EC	e1178	
36	MLG 1	130.2729	-40.8669	EC	e1112								

**Table B3.** Derived physical parameters of open cluster candidates.

Name	$\alpha$ (J2000) °	$\delta$ (J2000) °	Dist <sub>phot</sub> kpc	Dist <sub>Gaia</sub> kpc	E( $J-K_S$ ) mag	Mass M <sub>☉</sub>	Age Myr	$\mu_\alpha \cos \delta$ mas yr <sup>-1</sup>	$\mu_\delta$ mas yr <sup>-1</sup>	[Fe/H] dex
Bica 372	112.7083	-19.2572	3.1 $\pm$ 0.27	3.1 $\pm$ 1.6	0.57 $\pm$ 0.04	2990 $\pm$ 511	20 $\pm$ 3	-1.48 $\pm$ 0.88	1.68 $\pm$ 1.20	-0.70 $\pm$ 0.14
Bica 376	112.9625	-19.2964	2.3 $\pm$ 0.05	2.4 $\pm$ 1.1	0.19 $\pm$ 0.04	865 $\pm$ 343	275 $\pm$ 13	-2.00 $\pm$ 0.53	2.34 $\pm$ 0.51	0.07 $\pm$ 0.02
Bica 377	112.9958	-19.2986	3.8 $\pm$ 0.31	2.3 $\pm$ 1.2	0.43 $\pm$ 0.06	5290 $\pm$ 2160	375 $\pm$ 13	-1.70 $\pm$ 1.12	1.99 $\pm$ 1.10	0.10 $\pm$ 0.02
Bica 378	112.9833	-19.3292	2.2 $\pm$ 0.02	2.5 $\pm$ 1.2	0.18 $\pm$ 0.04	320 $\pm$ 109	250 $\pm$ 13	-1.83 $\pm$ 0.62	2.10 $\pm$ 0.84	-0.07 $\pm$ 0.03
Bica 387	120.6375	-34.5042	2.9 $\pm$ 0.14	3.0 $\pm$ 1.4	0.27 $\pm$ 0.04	1120 $\pm$ 442	350 $\pm$ 25	-2.29 $\pm$ 0.56	2.84 $\pm$ 0.44	0.20 $\pm$ 0.05
Bica 405	140.6500	-51.9400	3.2 $\pm$ 0.03	3.1 $\pm$ 0.6	0.44 $\pm$ 0.02	1640 $\pm$ 215	650 $\pm$ 25	-4.12 $\pm$ 0.63	3.54 $\pm$ 0.61	0.16 $\pm$ 0.02
Bica 408	141.3833	-52.1133	3.7 $\pm$ 0.52	3.5 $\pm$ 1.5	0.57 $\pm$ 0.06	3620 $\pm$ 1440	30 $\pm$ 3	-3.70 $\pm$ 0.85	3.12 $\pm$ 0.74	0.10 $\pm$ 0.02
Bica 422	159.6250	-58.3133	2.0 $\pm$ 0.03	1.6 $\pm$ 0.9	0.13 $\pm$ 0.04	884 $\pm$ 308	500 $\pm$ 25	-6.17 $\pm$ 1.45	2.81 $\pm$ 1.38	-0.23 $\pm$ 0.10
Cmg 218	126.5792	-40.8108	0.8 $\pm$ 0.07	1.3 $\pm$ 0.7	0.24 $\pm$ 0.06	538 $\pm$ 165	175 $\pm$ 13	-2.45 $\pm$ 0.78	3.18 $\pm$ 1.56	-0.58 $\pm$ 0.32
Cmg 398	149.5917	-56.3703	2.0 $\pm$ 0.21	2.3 $\pm$ 0.9	0.53 $\pm$ 0.04	530 $\pm$ 259	70 $\pm$ 10	-3.47 $\pm$ 0.45	3.39 $\pm$ 0.65	0.16 $\pm$ 0.02
Cmg 405	149.7500	-56.8617	2.7 $\pm$ 0.36	2.3 $\pm$ 1.1	0.48 $\pm$ 0.04	1570 $\pm$ 578	175 $\pm$ 25	-5.23 $\pm$ 0.82	3.51 $\pm$ 1.35	0.18 $\pm$ 0.02
Cmg 406	149.8125	-56.9128	2.6 $\pm$ 0.46	2.3 $\pm$ 1.0	0.48 $\pm$ 0.06	2100 $\pm$ 844	60 $\pm$ 5	-5.59 $\pm$ 1.28	3.59 $\pm$ 1.60	0.27 $\pm$ 0.02
DBSB 9	112.9458	-19.3672	2.1 $\pm$ 0.15	2.1 $\pm$ 0.6	0.25 $\pm$ 0.04	1340 $\pm$ 400	600 $\pm$ 50	-2.14 $\pm$ 0.26	2.49 $\pm$ 0.60	0.16 $\pm$ 0.02
Maj 107	127.3083	-41.1800	2.8 $\pm$ 0.07	2.9 $\pm$ 1.1	0.45 $\pm$ 0.04	1280 $\pm$ 397	45 $\pm$ 3	-2.79 $\pm$ 0.32	3.21 $\pm$ 0.52	0.07 $\pm$ 0.03
Teu 215	116.3750	-20.8306	2.2 $\pm$ 0.06	2.2 $\pm$ 0.9	0.12 $\pm$ 0.04	12000 $\pm$ 3520	2500 $\pm$ 120	-1.81 $\pm$ 0.79	1.95 $\pm$ 1.24	-0.23 $\pm$ 0.05
CL 204	128.4500	-44.4483	0.7 $\pm$ 0.01	3.0 $\pm$ 1.2	0.18 $\pm$ 0.04	397 $\pm$ 59	7500 $\pm$ 120	-2.71 $\pm$ 0.42	3.40 $\pm$ 0.71	-1.28 $\pm$ 0.05
CL 207	145.6292	-52.4306	2.5 $\pm$ 0.03	2.8 $\pm$ 1.2	0.55 $\pm$ 0.02	1030 $\pm$ 119	500 $\pm$ 25	-4.42 $\pm$ 0.57	3.53 $\pm$ 0.50	0.23 $\pm$ 0.02
CL 208	148.5833	-56.4233	2.8 $\pm$ 0.05	2.9 $\pm$ 1.2	0.51 $\pm$ 0.02	1960 $\pm$ 231	200 $\pm$ 13	-4.74 $\pm$ 0.92	3.36 $\pm$ 0.62	0.20 $\pm$ 0.02

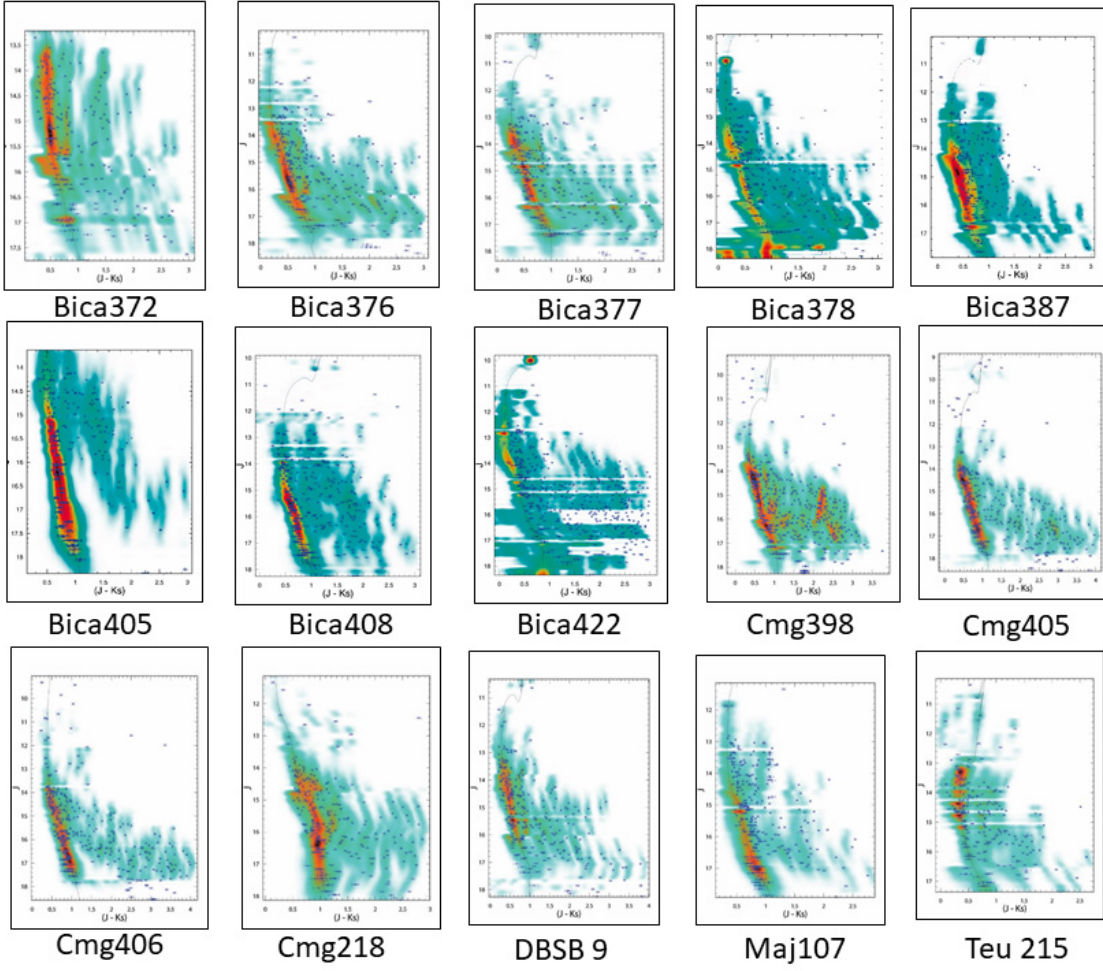


**Figure B1.** VVVX  $((J - K_s), J)$  Hess color magnitude diagrams for some known open clusters from [Bica et al. \(2019\)](#) catalog.